

Optimization of Far-field Radiation from Impedance-Loaded Nanoloops Accelerated by an Exact Analytical Formulation

Jogender Nagar, *Student Member, IEEE*, Ryan J. Chaky, *Student Member, IEEE*,
Mario F. Pantoja, *Senior Member, IEEE*, Arnold F. McKinley, and Douglas H. Werner, *Fellow, IEEE*

Abstract— Impedance loading is a common technique traditionally used in the RF to enhance the performance of an antenna, but its application in the optical regime is not as rigorously studied. This is mainly due to a lack of exact analytical expressions that can be used to rapidly predict the radiation properties of loaded nanoantennas. This paper will derive a set of useful analytical expressions for the far-field radiation properties of loop antennas loaded with an arbitrary number of lumped impedances that are valid from the RF to optical regimes. The analytical expressions will be validated with full-wave solvers and can be evaluated more than 100x faster. The ability to perform such rapid evaluations enables, for the first time, large-scale single- and multi-objective optimizations. A series of optimizations reveal that electrically small super-directive antennas can be achieved at a variety of far field angles through capacitive loading, paving the way for a pattern reconfigurable antenna. In addition, gains of greater than 3 dB can be achieved for electrically small antennas over a fractional bandwidth of 28%. Finally, it is shown that impedance loading can be used to achieve circularly polarized radiation from a single loop.

Index Terms— Antenna theory, Loop antennas, Optimization, Nanotechnology, Submillimeter wave technology.

I. INTRODUCTION

THE antenna operating in the RF and optical regimes is an enabling component in a wide variety of applications, including radar systems and solar energy harvesting [1, 2]. Loading an antenna with multiple impedances can alter its operating characteristics to suit a particular application [3]. The ability to tune these impedances leads to reconfigurable antennas which can adapt based on changing system requirements or the environment [4]. Exact analytical expressions for the radiation properties of impedance-loaded antennas would allow insight into the underlying physical behavior of these structures and also enable extremely fast parameter sweeps and even global optimizations.

The method of moments was generalized by Harrington in 1967 to include the effects of impedance loading for straight-

wire antennas [5]. Analytic expressions for the current distribution, input impedance and radiation properties of impedance-loaded dipoles were later derived, giving better insight into the effects of impedance loading [6]. These loading techniques were then used to greatly improve the performance of conventional dipoles, including enhancing the efficiency of a short dipole [7] and achieving a traveling-wave condition [8]. Through the use of PIN diodes, varactor diodes and MEMS devices, dipole antennas were made reconfigurable in terms of the frequency range of operation [9] and the radiation pattern [10].

In addition to the RF regime, the design of nanoantennas for use anywhere from the optical to terahertz regimes is of increasing interest [11]. At these frequencies, metals start to exhibit dispersion and loss, which can have a dramatic effect on the radiation properties of such nanoantennas [2]. There is a large amount of literature available on the analysis of linear dipole nanowire antennas [12, 13]. In analogy with RF antennas, nanoscale circuit elements would allow improved performance and reconfigurability in the optical regime. While lumped circuit elements at these frequencies are not readily available, they can approximately be realized through positive permittivity nanoparticles for capacitive loading and negative permittivity nanoparticles for inductive loading [14, 15]. Alternately, core-shell nanoparticles could be employed as a tunable nanocircuit element which can be treated analytically [16]. These structures can be used to tune the input impedance and radiation properties of optical nanodipoles [17].

While a large amount of literature exists on the theory, analysis and design of impedance loaded dipoles in the RF and optical regimes, much less work exists on the loop antenna despite its simplicity, versatility and utility [1]. Initial analytical work on impedance loaded loops focused on positive and negative resistive loads implemented by Esaki diodes. [18]. It has been shown through full-wave simulation that impedance loading can be used to achieve a uniform traveling-wave current distribution [19] or an omni-directional left-handed circularly

Paper submitted for review on 03/20/2018. The authors would like to acknowledge the Spanish Ministry of Education - Commission Fulbright Program “Salvador de Madariaga” (PRX14/00320) for sponsoring the joint research collaboration. This work has also been partially financed by the Spanish and Andalusian research programs TEC2013-48414-C3-01 and P12-TIC-1442 as well as by the Center for Nanoscale Science, an NSF Materials Research Science and Engineering Center, under the award DMR-1420620.

J. Nagar, R. Chaky and D. H. Werner are with the Electrical Engineering Department, The Pennsylvania State University, University Park, PA 16802, USA (e-mail: jun16e3@psu.edu, by15088@psu.edu, and dhw@psu.edu).

M. F. Pantoja is with the Electrical Engineering Department, University of Granada, Granada, Spain (e-mail: mario@ugr.es).

A. F. McKinley is with the Electronic and Electrical Engineering Department at University College London (email: arni.mckinley@ucl.ac.uk)

polarized radiation pattern [20]. Optical nanoloops are extremely promising with a wide variety of applications including sensing [21] and light-trapping in solar cells [22]. Due to the complexity of the integrals that must be solved, fully analytical expressions for the radiation properties of impedance-loaded loops valid from the RF to optical regimes have not been developed. This paper will remedy that by providing simple and efficient analytical expressions for the far-zone fields, the directivity and the gain.

Section II will show the derivation of exact analytical expressions for the radiation properties of impedance-loaded loop antennas. Section III validates these results by comparing the analytical theory implemented in MATLAB [23] with the full-wave solvers FEKO [24] and HFSS [25]. The MATLAB code is at least 100x faster while only requiring 1.5% of the peak memory required by FEKO. Then, the utility of these expressions will be demonstrated in Section IV through a variety of parametric sweeps and optimizations. First, capacitive loading will be employed to achieve electrically small superdirective radiation over a prescribed set of far field angles. Several of these solutions will be studied in detail to understand the physical effects of impedance loading. Then it will be shown that reactive loading can be used to convert a linearly polarized loop to one which is circularly polarized. For a particular optimization, more than five days would be required if the full-wave solver FEKO is employed, while only 80 minutes are needed when the analytical representation derived in this paper is used.

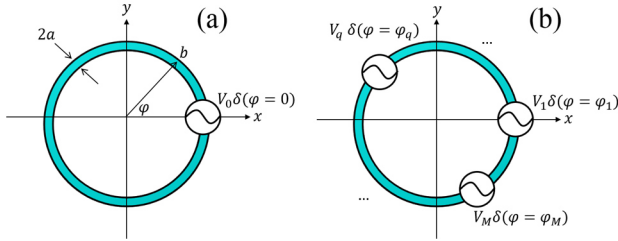


Fig. 1. (a) Geometry of the circular loop with wire radius a and loop radius b where a delta-gap voltage source with voltage V_0 is placed at $\varphi = 0$. (b) Geometry of the circular loop with M voltage sources where the q 'th source with voltage V_q placed at $\varphi = \varphi_q$.

II. THEORETICAL FORMULATION

Fig. 1 (a) shows the geometry of a circular loop with wire radius a and loop radius b which satisfies the thin-wire approximation ($a^2 \ll b^2, a \ll \lambda$). The parameter $\Omega = 2 \ln(2\pi b/a)$ will be adopted as a useful measure to characterize the wire thickness. In addition, a unit-less quantity $k_b = \frac{2\pi b}{\lambda}$, which is related to the electrical circumference of the loop, will be utilized throughout the derivation. An infinitesimal voltage source with voltage V_0 is placed at $\varphi = 0$. The resulting current distribution can be expressed as a Fourier series with modal coefficients I'_m where the prime is used to signify this expression is valid for lossy materials:

$$I(\varphi) = \sum_{m=-\infty}^{\infty} I'_m e^{jm\varphi} \quad (1)$$

This expression can be rewritten in terms of modal admittances Y'_m such that:

$$I(\varphi) = V_0 \left[\sum_{m=-\infty}^{\infty} Y'_m e^{jm\varphi} \right] \quad (2)$$

$$Y'_0 = [j\pi\eta_0 a_0 + (b/a)Z_s]^{-1}$$

$$Y'_m = [j\pi\eta_0(a_m/2) + (b/a)(Z_s/2)]^{-1}$$

where η_0 is the characteristic impedance of free space, a_m are coefficients explicitly defined in [26], and Z_s is the characteristic impedance of the metallic wire [27]. Given the modal current coefficients I'_m the far-zone electric field components can be expressed in spherical coordinates (θ, ϕ) as [28]:

$$E_\theta = \frac{\eta_0 e^{-jk_0 r} \cot \theta}{r} \sum_{m=1}^{\infty} m j^m I'_m \sin(m\varphi) J_m(w)$$

$$E_\varphi = -\frac{\eta_0 e^{-jk_0 r} k_b}{r} \sum_{m=0}^{\infty} \epsilon_m j^m I'_m \cos(m\varphi) J'_m(w) \quad (3)$$

$$\epsilon_m = \begin{cases} 1/2 & m = 0 \\ 1 & m \neq 0 \end{cases}$$

where $w = k_b \sin \theta$, $k_0 = \frac{2\pi}{\lambda}$, J_m is a Bessel function of the first kind, and J'_m is the derivative of the Bessel function with respect to its argument. Note that this expression makes the assumption that the current is symmetric and therefore $I'_m = I'_{-m}$.

Fig. 1 (b) illustrates the geometry of a loop with multiple loads placed at $\varphi = \varphi_q$ for $q = 1, \dots, M$. Each load has an associated Thevenin equivalent voltage V_q and impedance Z_q . The derivation of the total current will follow that of [29] but will employ standard matrix notation instead of Einstein summation notation, making the formulation much easier to implement in MATLAB. Note that a tilde will be used to differentiate quantities which include the effect of impedance loads. The total current is given by:

$$\tilde{I}(\varphi) = \sum_{q=1}^M \left[\sum_{m=-\infty}^{\infty} Y'_m e^{jm(\varphi-\varphi_q)} \right] \{V_q - Z_q I(\varphi_q)\} \quad (4)$$

If the current at each port $I(\varphi_q)$ is known, the total current at any location can be computed. To calculate $I(\varphi_q)$, a matrix equation will be obtained by first considering $I(\varphi_p)$ for $p = 1, \dots, M$:

$$\tilde{I}(\varphi_p) = \sum_{q=1}^M \left[\sum_{m=-\infty}^{\infty} Y'_m e^{jm(\varphi_p-\varphi_q)} \right] \{V_q - Z_q I(\varphi_q)\} \quad (5)$$

To formulate the matrix equation, $\tilde{\mathbf{I}}$ will be defined as an $N \times 1$ current vector where $\tilde{I}_q = I(\varphi_q)$ and $\tilde{\mathbf{V}}$ is the $M \times 1$ voltage vector with components equal to the voltage at each port V_q . Let

$\tilde{\mathbf{Y}}$ be an $M \times M$ admittance matrix with components:

$$\tilde{Y}_{pq} = Y'_m e^{jm(\varphi_p - \varphi_q)} \quad (6)$$

$$= \frac{1}{2\pi} \left[\sum_{m=-\infty}^{\infty} Y'_m \int_{-\pi}^{\pi} e^{-jn\varphi} e^{jm(\varphi - \varphi_1)} \dots \sum_{m=-\infty}^{\infty} Y'_m \int_{-\pi}^{\pi} e^{-jn\varphi} e^{jm(\varphi - \varphi_N)} \right] \tilde{\mathbf{G}} \quad (14)$$

Also, let $\tilde{\mathbf{Z}}$ be an $M \times M$ impedance matrix whose off-diagonal components are zero and diagonal components given by the impedance at port $\tilde{Z}_{qq} = Z_q$. Finally, we define $\tilde{\mathbf{X}}$ to the $M \times M$ identity matrix. Using these definitions, (5) can be formulated as a matrix equation in terms of the unknown $\tilde{\mathbf{I}}$:

$$(\tilde{\mathbf{X}} + \tilde{\mathbf{Y}}\tilde{\mathbf{Z}})\tilde{\mathbf{I}} = \tilde{\mathbf{Y}}\tilde{\mathbf{V}} \quad (7)$$

The current vector can then be calculated as:

$$\tilde{\mathbf{I}} = (\tilde{\mathbf{X}} + \tilde{\mathbf{Y}}\tilde{\mathbf{Z}})^{-1} \tilde{\mathbf{Y}}\tilde{\mathbf{V}} = \tilde{\mathbf{F}}^{-1} \tilde{\mathbf{Y}}\tilde{\mathbf{V}} \quad (8)$$

where the auxiliary matrix $\tilde{\mathbf{F}}$ is defined as $\tilde{\mathbf{X}} + \tilde{\mathbf{Y}}\tilde{\mathbf{Z}}$. Finally, the current at any point given by (4) can be written in matrix notation as:

$$\tilde{I}(\varphi) = \tilde{\mathbf{A}}(\tilde{\mathbf{V}} - \tilde{\mathbf{Z}}\tilde{\mathbf{I}}) = \tilde{\mathbf{A}}(\tilde{\mathbf{V}} - \tilde{\mathbf{Z}}\tilde{\mathbf{F}}^{-1}\tilde{\mathbf{Y}}\tilde{\mathbf{V}}) \quad (9)$$

where $\tilde{\mathbf{A}}$ is a $1 \times N$ row vector whose components are:

$$\tilde{A}_q = \sum_{m=-\infty}^{\infty} Y'_m e^{jm(\varphi - \varphi_q)} \quad (10)$$

If we define $\tilde{\mathbf{G}} = \tilde{\mathbf{V}} - \tilde{\mathbf{Z}}\tilde{\mathbf{F}}^{-1}\tilde{\mathbf{Y}}\tilde{\mathbf{V}}$, then we obtain:

$$\tilde{I}(\varphi) = \tilde{\mathbf{A}}\tilde{\mathbf{G}} \quad (11)$$

Since the far-field quantities given in (3) are expressed in terms of the modal current components I'_m , it is necessary to derive the corresponding components for the loaded case represented by \tilde{I}_m . Expressed in terms of these modal contributions, the current when considering impedance loads is given by:

$$\tilde{I}(\varphi) = \sum_{m=-\infty}^{\infty} \tilde{I}_m e^{jm\varphi} \quad (12)$$

Setting (11) equal to (12) and expressing each component of $\tilde{\mathbf{A}}$ using (10), we arrive at:

$$= \left[\sum_{m=-\infty}^{\infty} Y'_m e^{jm(\varphi - \varphi_1)} \dots \sum_{m=-\infty}^{\infty} Y'_m e^{jm(\varphi - \varphi_N)} \right] \tilde{\mathbf{G}} \quad (13)$$

Multiplying both sides by $\frac{1}{2\pi} e^{-jn\varphi}$ and integrating from $-\pi$ to π we obtain:

Using the orthogonality of the complex exponential functions we arrive at our final expression for \tilde{I}_m :

$$\tilde{I}_m = Y'_m [e^{-jm\varphi_1} \dots e^{-jm\varphi_N}] \tilde{\mathbf{G}} \quad (15)$$

In this case the current may no longer be symmetric and \tilde{I}_m and \tilde{I}_{-m} may not be the same. Hence, the far-zone fields may be expressed as:

$$\tilde{E}_\theta = -j \frac{\eta_0 e^{-jk_0 r} \cot \theta}{2r} \sum_{m=1}^{\infty} m j^m \{ \tilde{I}_m e^{jm\varphi} - \tilde{I}_{-m} e^{-jm\varphi} \} J_m(w)$$

$$\tilde{E}_\varphi = -\frac{\eta_0 e^{-jk_0 r} k_b}{2r} \sum_{m=0}^{\infty} \epsilon_m j^m \{ \tilde{I}_m e^{jm\varphi} + \tilde{I}_{-m} e^{-jm\varphi} \} J'_m(w) \quad (16)$$

The radiated power can be found by integrating the fields given in (16), resulting in:

$$\tilde{P}_r(k_b) = \frac{\eta_0 \pi k_b^2}{2} |V_0|^2 \tilde{T}(k_b) \quad (17)$$

$$\tilde{T}(k_b) = \sum_{m=0}^{\infty} \epsilon_m \{ |\tilde{Y}_m|^2 + |\tilde{Y}_{-m}|^2 \} \left[\frac{1}{2} Q_{m-1, m-1}^{(1)}(k_b) + \frac{1}{2} Q_{m+1, m+1}^{(1)}(k_b) - \frac{m^2}{k_b^2} Q_{mm}^{(1)}(k_b) \right] \quad (18)$$

where $Q_{mn}^{(p)}(x)$ are the Q -type integrals defined in [30] and $\tilde{Y}_m = \tilde{I}_m / V_0$. The radiation intensity at (θ, φ) is given in terms of normalized far-zone electric fields $\tilde{E}_\theta^0 = r e^{jk_0 r} \tilde{E}_\theta$, $\tilde{E}_\varphi^0 = r e^{jk_0 r} \tilde{E}_\varphi$, as:

$$\tilde{U}(\theta, \varphi) = \frac{1}{2\eta_0} \left[|\tilde{E}_\theta^0|^2 + |\tilde{E}_\varphi^0|^2 \right] \quad (19)$$

where, from (16):

$$|\tilde{E}_\theta^0|^2 = \frac{|V_0|^2 \eta_0^2 \cot^2 \theta}{4} \sum_{m=-\infty}^{\infty} \sum_{n=-\infty}^{\infty} \left[mn (-1)^n j^{m+n} \tilde{Y}_m \tilde{Y}_n^* e^{j(m-n)\varphi} \cdot \right]$$

$$|\tilde{E}_\varphi^0|^2 = \frac{|V_0|^2 \eta_0^2 k_b^2}{4} \sum_{m=-\infty}^{\infty} \sum_{n=-\infty}^{\infty} \left[(-1)^n j^{m+n} \tilde{Y}_m \tilde{Y}_n^* e^{j(m-n)\varphi} \cdot \right]$$

$$\left[\frac{J_m(k_b \sin \theta) J_n(k_b \sin \theta)}{J'_m(k_b \sin \theta) J'_n(k_b \sin \theta)} \right] \quad (20)$$

The directivity is given by:

$$\tilde{D}(\theta, \varphi) = \frac{4\pi \tilde{U}(\theta, \varphi)}{\tilde{P}_r(k_b)} \quad (21)$$

Where an exact expression can be obtained by substituting (17)-(20) into (21). In order to calculate the gain, the loss resistance and input radiation resistance must be determined. The loss resistance is expressed as:

$$\tilde{R}_{loss} = \frac{b \operatorname{Re}(Z_s)}{a} \frac{1}{|\tilde{I}_{in}|^2} \int_0^{2\pi} |\tilde{I}(\varphi)|^2 d\varphi \quad (22)$$

Plugging (12) into (22) and using the modal admittances results in a more convenient form for the loss resistance:

$$\tilde{R}_{loss} = \operatorname{Re}(Z_s) \frac{b}{a} |\tilde{z}_{in}|^2 \sum_{m=0}^{\infty} \epsilon_m \{ |\tilde{Y}_m|^2 + |\tilde{Y}_{-m}|^2 \} \quad (23)$$

The input radiation resistance is given by:

$$\tilde{R}_{rad,in} = \frac{2\tilde{P}_r(k_b)}{|\tilde{I}_{in}|^2} = \frac{2\tilde{P}_r(k_b) |\tilde{z}_{in}|^2}{|V_0|^2} \quad (24)$$

Substituting (17) into (24) results in:

$$\tilde{R}_{rad,in} = k_b^2 \pi \eta_0 |\tilde{z}_{in}|^2 \tilde{\tau}(k_b) \quad (25)$$

Finally, the gain may be obtained from:

$$\tilde{G}(\theta, \varphi) = e' \tilde{D}(\theta, \varphi) = \frac{\tilde{R}_{rad,in}}{\tilde{R}_{rad,in} + \tilde{R}_{loss}} \tilde{D}(\theta, \varphi) \quad (26)$$

III. VALIDATION

In order to validate the derivations, the solutions represented by (4)-(26) were implemented in MATLAB and compared to the full-wave solver FEKO. Efficiency tests were performed on a Dual Intel Xeon Processor with 10 cores. FEKO was run in parallel mode utilizing all 10 cores, while the MATLAB code used only a single core. As a simple example, a 3000 nm circumference nanoloop comprised of gold with $\Omega = 8$ was evaluated at 51 frequency points in the range $k_b \in [0.1, 2.5]$. The material prescription given in [29] was used to represent the refractive index of gold. A capacitive load placed at $\phi_L = 180^\circ$ was modeled in MATLAB as a lumped impedance and in FEKO as a dielectric slab using the approach described in [14]. Table I provides a summary of the computational resources required for each method. As can be seen, the full-wave simulation method took more than an hour to complete, while the analytical method performed in MATLAB took approximately 42 seconds. Note that if FEKO were run in serial mode (*i.e.* using only one core), the solution time would be more than 12 hours. The long simulation times required by FEKO make large parameter sweeps and optimizations intractable while, on the other hand, the extremely rapid evaluations in MATLAB enable such studies to be performed for the first time. There is also a savings in memory usage. FEKO requires 1.8 GB while the MATLAB code only requires 26 MB of memory. In summary, the analytical method is over 100x faster while only requiring 1.5% of the memory.

Method	Time	Memory
Full-wave	1.26 hours	1.83 GB
Analytical	42 seconds	26 MB

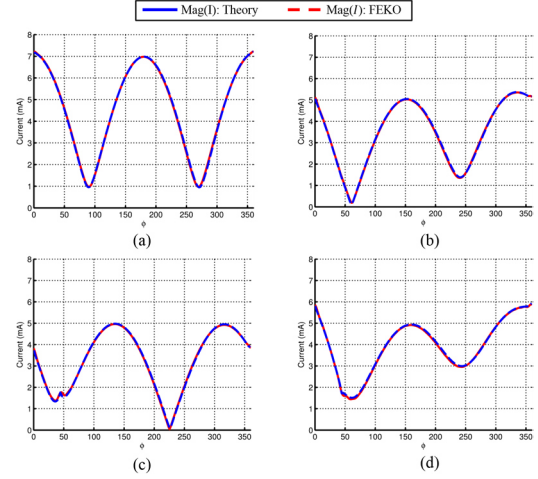


Fig. 2. Comparison between the theory and FEKO for the magnitude of the current on (a) an unloaded PEC loop and a loaded PEC loop with (b) $r = 1$, (c) $l_\mu = 1$ and (d) $l_\epsilon = 1$.

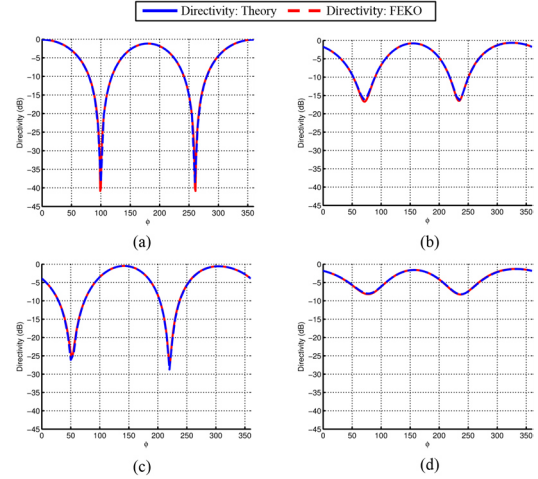


Fig. 3. Comparison between the theory and FEKO for the directivity corresponding to (a) an unloaded PEC loop and a loaded PEC loop with (b) $r = 1$, (c) $l_\mu = 1$ and (d) $l_\epsilon = 1$.

To simplify discussion of the results for PEC loops, unit-less parameters r , l_ϵ , and l_μ for the resistance, capacitance and inductance, respectively, will be used to describe a load impedance [29]:

$$Z_L \equiv \eta_0 \left[r + j \left(k_b l_\mu - \frac{1}{k_b l_\epsilon} \right) \right] \quad (27)$$

Fig. 2 shows a comparison between the theory and the results from FEKO for the magnitude of the current at the voltage source corresponding to a thin-wire PEC loop with $\Omega = 12$ at the first resonance $k_b = 1.06$. Fig. 2 (a) shows the results for the unloaded loop, while results for a loaded loop with a load placed at $\phi = 45^\circ$ are shown for (b) $r = 1$, (c) $l_\mu = 1$ and (d) $l_\epsilon = 1$. As can be seen, there is excellent agreement between the theory and FEKO. Fig. 3 shows a comparison of the

directivity versus ϕ where $\theta = 90^\circ$ for these same cases; again, the agreement is excellent. Note that a thin-wire approximation is employed in FEKO to model the PEC loop antenna for which a load with an explicitly defined complex impedance can be specified.

Next, similar comparisons will be performed for a gold nanoloop. In this case most commercial solvers do not support the use of a thin-wire model nor can a lumped load be explicitly defined. In order to model a lumped capacitance and inductance, slabs with the material properties $Re\{\epsilon_r\} > 0$ and $Re\{\epsilon_r\} < 0$ respectively, can be utilized [14]. To model a lumped resistance, a material with either $\sigma > 0$ or $Im\{\epsilon_r\} > 0$ can be used. In order to validate the derived expressions, slabs with the material properties $\epsilon_r = 12$, $\epsilon_r = -12$ and $\sigma = 1$ are used to model a lumped capacitance, inductance and resistance, respectively. While these materials may not be feasible in practice, they are useful for validation purposes. In the analytical code the lumped impedances are calculated by:

$$Z_L = -\frac{jd}{\omega\epsilon_0\epsilon_r\pi a^2} \quad \text{for reactive load} \quad (28)$$

$$Z_L = \frac{d}{\sigma\pi a^2} \quad \text{for resistive load}$$

where the thickness d is given by $2\pi b\left(\frac{\alpha}{360}\right)$ for a slab of angular width α . Moreover, a lossy dielectric can be modeled by a capacitance and conductance in parallel [31]. We note that FEKO cannot handle materials with a negative permittivity, so Ansys HFSS will be used for these comparisons. It has been found from experience that a thin slab of $\alpha = 2^\circ$ provides a good approximation to a lumped impedance. Thicker loops (*i.e.* smaller Ω) tend to work better as the effect of fringing in this case can be ignored [31]. The example considered for validation will be a gold loop with circumference 3000 nm and $\Omega = 8$ having identical lumped impedances placed at $\phi = 90^\circ$ and $\phi = 270^\circ$. The results will be plotted in terms of k_b over the range [0,1,1].

Fig. 4 shows a comparison between the theory and HFSS for the magnitude of the current at the voltage source for an

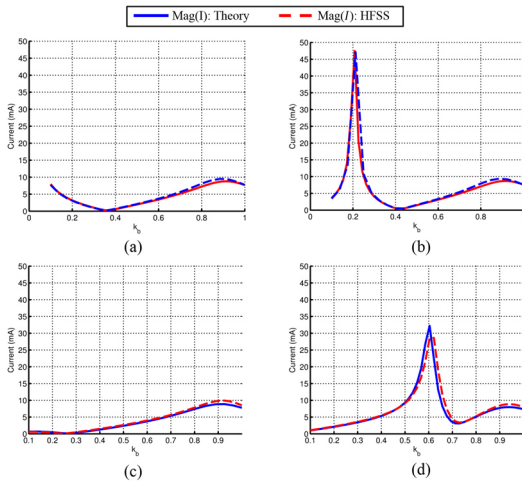


Fig. 4. Comparison between the theory and HFSS for the magnitude of the current on (a) an unloaded gold loop and a loaded gold loop with (b) $\epsilon_r = 12$, (c) $\epsilon_r = -12$ and (d) $\sigma = 1$.

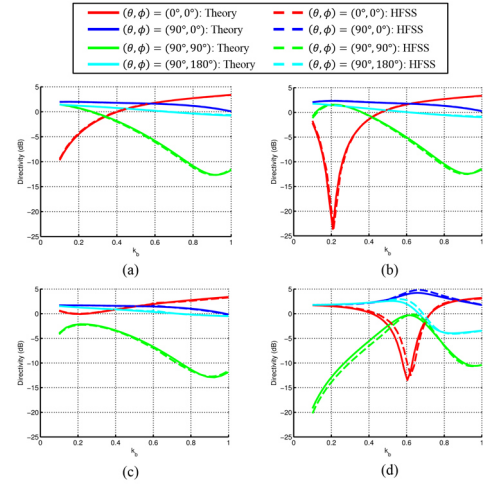


Fig. 5. Comparison between the theory and HFSS for the directivity corresponding to (a) an unloaded gold loop and a loaded gold loop with (b) $\epsilon_r = 12$, (c) $\epsilon_r = -12$ and (d) $\sigma = 1$.

unloaded loop in (a) as well as a loop loaded with a capacitance, inductance and resistance in (b), (c) and (d) respectively. As can be seen, the results are nearly identical. The capacitive and inductive loads have the most noticeable effect for lower frequencies, as expected from the analytical expressions. Interestingly, the capacitive loads induce a large current around $k_b = 0.2$, while the inductive load suppresses the current around this frequency. In the case of a resistive load, however, a large current is induced around $k_b = 0.5$. Fig. 5 shows a comparison between the theory and HFSS for the directivity at four angles of interest for the unloaded loop in (a), as well as the loop loaded with a capacitance, inductance and resistance in (b), (c) and (d) respectively. The unloaded case has a nearly omnidirectional pattern in the xy -plane at $k_b = 0.1$. As k_b increases to 1, the pattern gradually becomes nearly omnidirectional in the xz -plane. The capacitively loaded loop exhibits a bidirectional pattern along $(\theta, \phi) = (90^\circ, 0^\circ)$ and $(\theta, \phi) = (90^\circ, 180^\circ)$ at $k_b = 0.1$. The pattern is nearly omnidirectional in the xy -plane with extremely deep nulls in the broadside direction at $k_b = 0.2$, the same frequency where the current exhibits a peak. Above this frequency, the capacitively loaded loop behaves similarly to the unloaded case. In contrast, the inductively loaded loop is never omnidirectional in the xy -plane. The loop with the resistive load has extremely sharp nulls in the broadside directions at $k_b = 0.6$, the same frequency where the current exhibits a peak. Interestingly, the pattern is nearly unidirectional with a large directivity along $(\theta, \phi) = (90^\circ, 0^\circ)$ at around $k_b = 0.7$.

IV. OPTIMIZATION EXAMPLES

Due to the extremely fast function evaluations enabled by the analytical theory, large-scale parameter sweeps and global optimizations can be performed very rapidly. A variety of optimizations will be carried out here to highlight the utility of the analytical expressions. CMA-ES [32] has been found to be extremely effective in single-objective optimizations for electromagnetics problems [33-34]. In real-world engineering problems, there are often multiple conflicting objectives, with a classical example being size versus performance. A multi-objective optimizer (MOO) allows the engineer to view the

trade-offs between these objectives by providing a set of solutions called the Pareto Set (in design parameter space) or the Pareto Front (in objective space) [35]. BORG [36] has been found to be an effective MOO for problems in electromagnetics [37]. Even though BORG is very efficient, MOOs require more function evaluations to converge compared to single-objective optimizers. The extremely fast function evaluations which result from the analytical theory enables these MOOs to be performed efficiently.

First, a set of optimizations will be performed exploring the trade-off between directivity and the size, a subject which has received much recent theoretical attention [38]. Wheeler [39] defines an electrically small antenna (ESA) as one that fits within a volume smaller than a sphere defined by $k_b = \frac{2\pi b}{\lambda} < 1$. Chu [40] studied the tradeoffs between directivity and antenna size, but according to his equations the limit for superdirectivity approaches zero as k_b approaches zero. Geyi [41] re-formulated these expressions to be more suitable when describing ESAs. In his expressions the superdirective limit approaches the directivity of a Huygen's source as k_b approaches zero. It has recently been discovered theoretically that superdirectivity can be achieved by electrically small gold nanoloops [42-43]. A series of multi-objective studies revealed the trade-offs between directivity, gain and k_b for unloaded gold nanoloops [44]. This paper will extend these results by considering loaded nanoloops. Note that nanoloops can also be employed in a Yagi-Uda configuration to enhance directivity, resulting in a different set of tradeoffs [45-46].

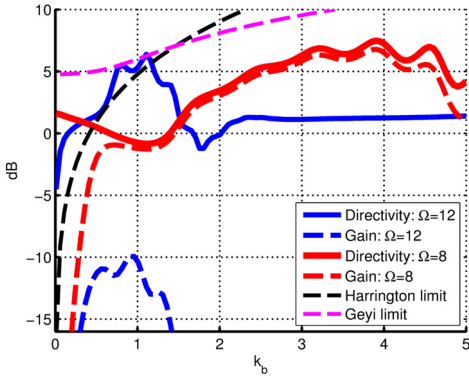


Fig. 6. Comparison of directivity and gain along $(\theta, \phi) = (90^\circ, 180^\circ)$ of a thin ($\Omega = 12$) and thick ($\Omega = 8$) circumference loop along with the Harrington and Geyi superdirective limits.

Fig. 6 shows one of the main results of [42-43], namely that a gold nanoloop with $b = 477 \text{ nm}$ exhibits high directivity along $(\theta, \phi) = (90^\circ, 180^\circ)$ over an extremely broad bandwidth, which is below the plasma frequency. As can be seen, a thin ($\Omega = 12$) loop exhibits superdirective performance according to the Geyi and Harrington limit at $k_b = 1.12$. Unfortunately, the gain at this frequency is very low due to an extremely poor efficiency. A thicker loop shifts the frequency range of high directivity to around $k_b = 4$ where the efficiency is remarkably high. Unfortunately for larger k_b the superdirective limit increases and this loop is no longer considered to be superdirective. Multi-objective studies have shown that a gold nanoloop could achieve superdirectivity

below $k_b = 1.5$ in terms of directivity but could never achieve supergain according to the Geyi limit [44]. A multi-objective study will be performed here using BORG with the goals of minimizing the electrical size k_b and maximizing the directivity as well as gain along various specified angles. The locations and capacitances of lumped impedance loads will be optimized, along with the radius of the loop b and the thickness measure Ω in the frequency range dictated by $k_b \in [0.1, 1]$ for directivity and $k_b \in [0.1, 3]$ for gain. The parameters will be constrained as follows: $b \in [47.7 \text{ nm}, 636 \text{ nm}]$, $\Omega \in [8, 12]$, $\phi_L \in [0^\circ, 360^\circ]$, $\alpha \in [0^\circ, 200^\circ]$. The loop radius and thickness measure limits were determined based on previous studies and are the same as those reported in [44]. The load can be placed anywhere around the loop, and the angular width of the silicon slab is allowed to vary over a large range. Note that the angular width is simply used to calculate the capacitance of a lumped load placed at ϕ_L based on (24); to implement such a load in practice the angular width can be scaled down and ϵ_r scaled up by the same factor.

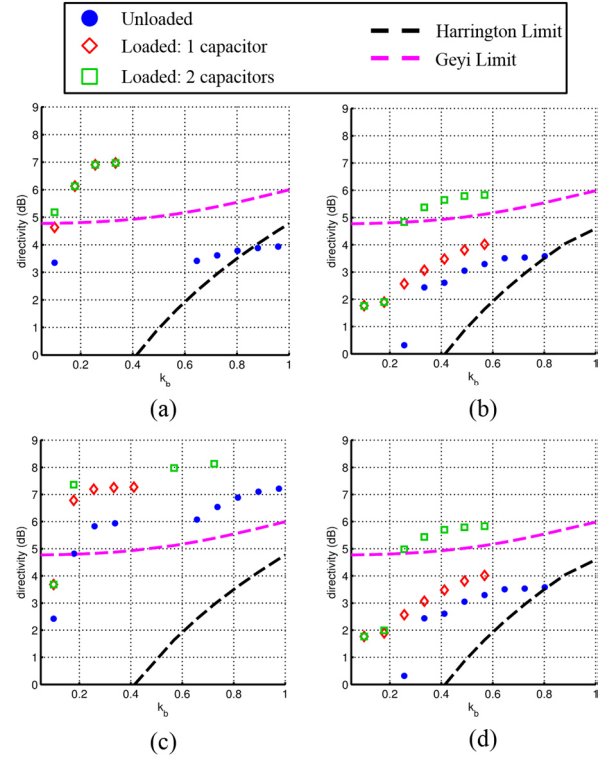


Fig. 7. Pareto fronts of an unloaded gold nanoloop and a gold nanoloop loaded with one or two capacitors. The objectives are minimizing k_b and maximizing directivity along (a) $(\theta, \phi) = (90^\circ, 0^\circ)$, (b) $(\theta, \phi) = (90^\circ, 90^\circ)$, (c) $(\theta, \phi) = (90^\circ, 180^\circ)$ and (d) $(\theta, \phi) = (90^\circ, 270^\circ)$.

Fig. 7 (a) shows the results of an optimization when one and two capacitive loads are considered with the following costs:

$$\begin{aligned} \text{COST}_1 &= \max\{\bar{D}(\theta, \phi)\} \\ \text{COST}_2 &= \min\{k_b\} \end{aligned} \quad (29)$$

As can be seen, the unloaded case cannot exceed the Geyi limit. Adding one capacitor greatly improves the directivity. While superdirectivity cannot quite be achieved at $k_b = 0.1$, it can be surpassed above this frequency. Adding two capacitors, however, allows the additional design freedom to exceed the Geyi limit over the entire frequency range of interest. It is instructive to examine the set of $k_b = 0.1$ solutions in more detail.

TABLE II
RESULTS OF OPTIMIZATION FOR $(\theta, \phi) = (90^\circ, 0^\circ)$

Number of Loads	b (nm)	Ω	$\phi_L(1)$ (deg)	$\alpha(1)$ (deg)	$\phi_L(2)$ (deg)	$\alpha(2)$ (deg)
0	506	11.5				
1	406	11.8	180	0.131		
2	72.5	8.8	60	10.65	300	10.65

As shown in Table II, the optimized solution for the unloaded case and the case with one load is an extremely thin nanoloop ($\Omega > 11$) with a loop radius of about 400-500 nm. However, the optimized solution for the case of two loads is a thick nanoloop with a loop radius of 72.5 nm. The optimized current magnitudes are shown in Fig. 8 (a). As expected, for maximum radiation along $(\theta, \phi) = (90^\circ, 0^\circ)$, the currents are symmetric in all cases. Fig. 8 (b), (c) and (d) shows the magnitudes of the modal currents for the optimized solutions with no loads, one load and two loads respectively. Both the unloaded solution and the single load solution have modal current magnitudes which decrease as the mode index increases. However, the solution with two loads shows a large contribution from the 2nd mode. This is impossible to achieve at this frequency with only a single load without breaking the symmetry of the current distribution.

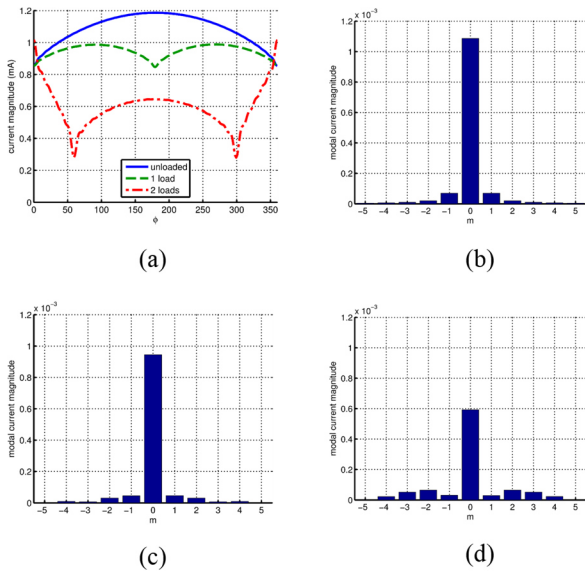


Fig. 8. Optimized results for maximum directivity along $(\theta, \phi) = (90^\circ, 0^\circ)$ at $k_b = 0.1$. (a) Current distributions for the optimized unloaded and loaded gold nanoloops. (b), (c) and (d) show the modal current magnitudes for the unloaded, loaded with one capacitor and loaded with two capacitor cases, respectively.

Fig. 7 (b) and (d) show the results of the optimization when considering the directions $(\theta, \phi) = (90^\circ, 90^\circ)$ and $(\theta, \phi) =$

$(90^\circ, 270^\circ)$, respectively. Note that the Pareto fronts are the same for both directions. For the unloaded case, the directivity is bidirectional. For the loaded configuration, the locations of the capacitors can be mirrored about the y -axis to swap between high directivity along $(\theta, \phi) = (90^\circ, 90^\circ)$ or $(\theta, \phi) = (90^\circ, 270^\circ)$. As can be seen, the unloaded case has very small directivities while the two capacitor loaded case can surpass the Geyi limit for electrically small antennas in the range $k_b \in [0.25, 1]$. Moreover, a single capacitor does not result in a large increase in directivity. In order to study the physics governing the observed loading effects, the two load solution at $k_b = 0.88$ will be considered in more detail. For this solution, $b = 589.7 \text{ nm}$, $\Omega = 10.1$, $\phi_L = [150^\circ, 199^\circ]$ and $\alpha = [20^\circ, 20^\circ]$. The unloaded configuration for these same loop dimensions will be considered as a basis for comparison. Fig. 9 shows a comparison of the real and imaginary components of the current and the magnitude of the modal admittances.

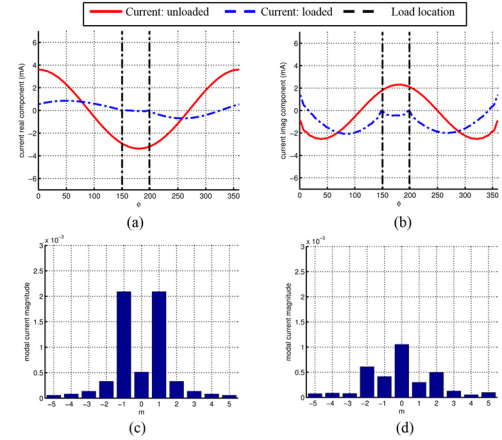


Fig. 9. Comparison of a loaded and unloaded gold nanoloop optimized for maximum directivity along $(\theta, \phi) = (90^\circ, 90^\circ)$ at $k_b = 0.88$. (a) Real and (b) imaginary components of the current. (c) and (d) show the modal current magnitudes for the unloaded and loaded cases, respectively.

Fig. 9 (a) and (b) shows the asymmetry in the current induced by the asymmetric capacitive loading. Fig. 9 (c) and (d) shows that the $m = -2$ mode is enhanced by the loading resulting in the highly directive pattern at $(\theta, \phi) = (90^\circ, 90^\circ)$. Mirroring the capacitors about the y -axis, *i.e.* placing them at $\phi_L = [161^\circ, 210^\circ]$ results in an enhancement of the $m = +2$ mode and a highly directive pattern at $(\theta, \phi) = (90^\circ, 270^\circ)$, while removing both capacitors leads to a bidirectional pattern along $(\theta, \phi) = (90^\circ, 0^\circ)$ and $(\theta, \phi) = (90^\circ, 180^\circ)$. Interestingly, this suggests that a pattern reconfigurable antenna could potentially be realized with this nanoloop using materials that changed permittivity based on some external stimulus, such as temperature or applied voltage [47]. The input impedance for this antenna is approximately $Z_{in} = 261 + j65$. Varying the gap for the load eliminates the imaginary part of the input impedance. Simulations performed in FEKO show that this has negligible impact on the far-field radiation properties.

Finally, Fig. 7 (c) shows the Pareto front corresponding to the direction $(\theta, \phi) = (90^\circ, 180^\circ)$. In this case, even though the unloaded case has extremely high directivity, adding loads can increase this value even further. Most of the optimized solutions

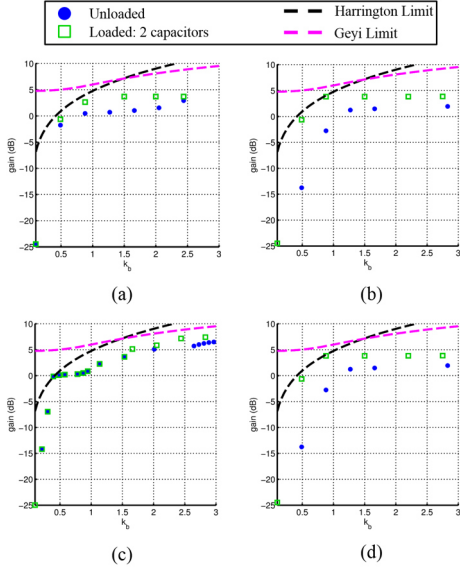


Fig. 10. Pareto fronts of an unloaded gold nanoloop and a gold nanoloop loaded with two capacitors. The objectives are minimizing k_b and maximizing gain along (a) $(\theta, \phi) = (90^\circ, 0^\circ)$, (b) $(\theta, \phi) = (90^\circ, 90^\circ)$, (c) $(\theta, \phi) = (90^\circ, 180^\circ)$ and (d) $(\theta, \phi) = (90^\circ, 270^\circ)$.

along all directions of interest resulted in fairly thin loops with $\Omega > 10$ except for when k_b is very small, less than approximately 0.5. While these solutions have very high directivity, they unfortunately suffer from poor efficiency and therefore low gain. Therefore, a second set of optimizations were run with the following costs:

$$\begin{aligned} COST_1 &= \max\{\bar{G}(\theta, \phi)\} \\ COST_2 &= \min\{k_b\} \end{aligned} \quad (30)$$

Only the case of two capacitive loads was considered. The results are shown in Fig. 10. Fig. 10 (a) and (c) show moderate and small improvement with the addition of loads, respectively, while Fig. 10 (b) and (d) show significant improvement for $k_b < 1$. The loaded solutions approach the Harrington limit but cannot quite reach the Geyi limit. The solution at $k_b = 0.88$ is

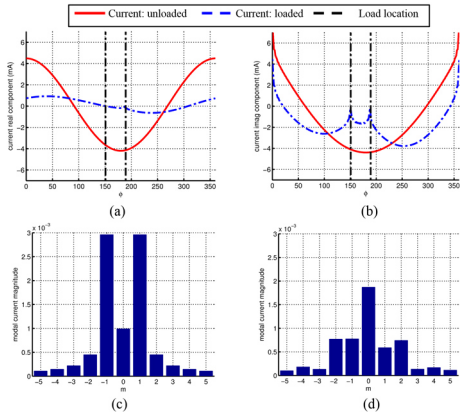


Fig. 11. Comparison of a loaded and unloaded gold nanoloop optimized for maximum gain along $(\theta, \phi) = (90^\circ, 90^\circ)$ at $k_b = 0.88$. (a) Real and (b) imaginary component of the current. (c) and (d) show the modal current magnitudes for the unloaded and loaded cases, respectively.

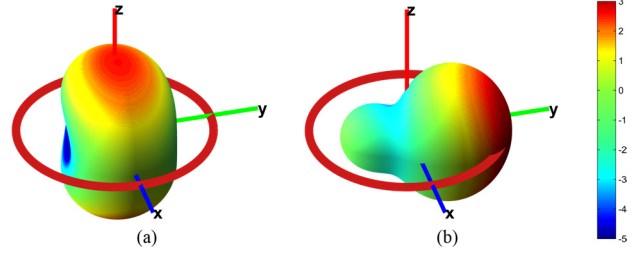


Fig. 12. Comparison of loaded and unloaded gold nanoloop optimized for maximum gain along $(\theta, \phi) = (90^\circ, 90^\circ)$ at $k_b = 0.88$. (a) Gain in dB of unloaded loop. (b) Gain in dB of loaded loop.

explored in more detail in Fig. 11. For this solution, $b = 636.67 \text{ nm}$, $\Omega = 8$, $\phi_L = [151^\circ, 189^\circ]$ and $\alpha = [200^\circ, 200^\circ]$. In practice, this loading configuration could be implemented by placing air gaps with $\alpha = 8.33^\circ$ at $\phi_L = [151^\circ, 189^\circ]$, which was validated in FEKO. The loaded currents shown in Fig. 11 look similar to those of Fig. 9. However, the efficiency in this case is nearly 80% while the efficiency for the optimized solution of Fig. 9 is only 10%. This is partly due to the fact that a thicker loop tends to result in higher efficiencies. However, simply making the loop of Fig. 9 thicker does not result in an appreciable increase in gain, suggesting the current distribution of Fig. 11 is finely tuned for high gain. The loads produce an extremely asymmetric current distribution, resulting in the radiation pattern changing from a bidirectional broadside to a unidirectional endfire pattern as shown in Fig. 12.

The final example will involve optimizing the polarization properties of a gold nanoloop. The electric field can be decomposed into left-hand circular polarization (LHP) and right-hand circular polarization (RHP) by the following equations [1]:

$$\begin{aligned} E_{LHP} &= \frac{1}{\sqrt{2}}(E_\theta - jE_\phi) \\ E_{RHP} &= \frac{1}{\sqrt{2}}(E_\theta + jE_\phi) \end{aligned} \quad (31)$$

where E_θ and E_ϕ are given in (3) for the unloaded case and (16) for the loaded case. The circularly polarized axial ratio is given by:

$$AR_{CP} = \frac{|E_{LHP}| + |E_{RHP}|}{|E_{LHP}| - |E_{RHP}|} \quad (32)$$

This quantity is often expressed using dB, where 0 dB corresponds to perfect circular polarization. An unloaded loop has theoretically perfect linear polarization ($AR_{CP} \rightarrow \infty$) in the broadside $\theta = 0^\circ$ and $\theta = 180^\circ$ directions. Fig. 13 (a) and (b) show the directivity and CP axial ratio in dB, respectively, for an unloaded loop with parameters $b = 477.5 \text{ nm}$ and $\Omega = 12$ evaluated at $k_b = 0.56$. As can be seen, the pattern is omnidirectional in the $\phi = 180^\circ$ plane and is linearly polarized in every direction where the directivity is greater than 0 dB. An optimization was performed using CMA-ES with the goal of obtaining circular polarization in the broadside direction, *i.e.* minimizing (32) in dB, similar to the study done in [48] for PEC loops. The optimal solution placed two loads at $\phi_L = 76.5^\circ$ and

$\phi_L = 88^\circ$ with angular widths $\alpha = 12.8^\circ$ and $\alpha = 10.7^\circ$ and permittivities of $\epsilon_r = 12$ and $\epsilon_r = -12$, respectively. As shown in Fig. 13 (c) and (d), the pattern is now slightly more bidirectional and circularly polarized in the two broadside directions.

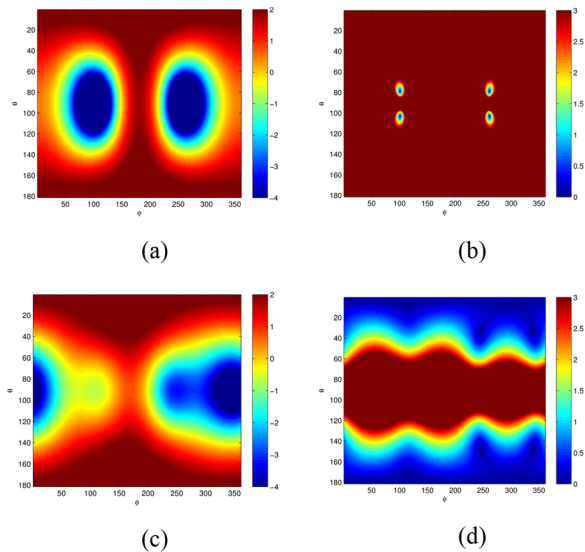


Fig. 13. (a) Directivity in dB and (b) axial ratio for circular polarization of an unloaded gold nanoloop. (c) Directivity and (d) axial ratio of a loaded gold nanoloop.

V. CONCLUSIONS

This paper presented exact, analytical expressions for the far-field radiation properties of circular loops with an arbitrary number of impedance loads valid from the RF to the optical regime. The expressions were implemented in MATLAB and validated against FEKO and HFSS for resistive, inductive and capacitive loads for both a PEC loop operating in the RF spectrum and a gold nanoloop operating in the optical regime. The analytical expressions, when implemented in MATLAB, can be evaluated over 100x faster than FEKO, enabling large-scale global single- and multi-objective optimizations. This was demonstrated through a series of optimization examples with the goal of achieving desirable radiation properties in the optical regime for particular applications. It was shown that two capacitive loads can result in a superdirective antenna along several targeted angles of interest. Moreover, gains of greater than 3 dB could be achieved for electrically small antennas over a fractional bandwidth of 28%. Finally, a combination of capacitive and inductive loading was shown to result in circularly polarized radiation in the broadside direction.

REFERENCES

- [1] C. A. Balanis, *Antenna Theory*. New York: Wiley, 1997.
- [2] L. Novotny and B. Hecht, *Principles of Nano-Optics*. Cambridge, UK: Cambridge University Press, 2012.
- [3] Y. Chen and C.-F. Wang, *Characteristic Modes: Theory and Applications in Antenna Engineering*. New Jersey: John Wiley & Sons, 2015.
- [4] J. T. Bernhard, "Reconfigurable antennas," *Synthesis Lectures on Antennas*, vol. 2, no. 1, pp. 1-66, 2007.

- [5] R. Harrington and J. Mautz, "Straight wires with arbitrary excitation and loading," *IEEE Transactions on Antennas and Propagation*, vol. 15, no. 4, pp. 502-515, July 1967.
- [6] S. Saoudy and M. Hamid, "Rigorous solution of a dipole antenna with lumped impedance loading," *Canadian Journal of Physics*, vol. 64, no. 11, pp. 1537-1545, November 1986.
- [7] R. Hansen, "Efficiency and matching tradeoffs for inductively loaded short antennas," *IEEE Transactions on Communications*, vol. 23, no. 4, pp. 430-435, April 1975.
- [8] D. Nyquist and Kun-Mu Chen, "The traveling-wave linear antenna with nondissipative loading," *IEEE Transactions on Antennas and Propagation*, vol. 16, no. 1, pp. 21-31, Jan 1968.
- [9] J. B. Ko and D. Kim, "A wideband frequency-tunable dipole antenna based on antiresonance characteristics," *IEEE Antennas and Wireless Propagation Letters*, vol. 16, pp. 3067-3070, 2017.
- [10] J. K. Ji, "Dual-band pattern reconfigurable antenna for wireless MIMO applications," *ICT Express*, vol. 2, no. 4, pp. 199-203, August 2018.
- [11] P. Biagioni, J.-S. Huang, and B. Hecht, "Nanoantennas for visible and infrared radiation," *Rep. Prog. Phys.*, vol. 75, pp. 024402/1-40, Jan. 2012.
- [12] P. Mühlshlegel, H.-J. Eisler, O. J. F. Martin, B. Hecht, and D. W. Pohl, "Resonant optical antennas," *Science*, vol. 308, no. 5728, pp. 1607-1609, June 2005.
- [13] P. J. Schuck, D. P. Fromm, A. Sundaramurthy, G. S. Kino, and W. E. Moerner, "Improving the mismatch between light and nanoscale objects with gold bowtie nanoantennas," *Phys. Rev. Lett.*, vol. 94, no. 1, pp. 017402/1-4, Jan. 2005.
- [14] N. Engheta, "Circuits with light at nanoscales: Optical nanocircuits inspired by metamaterial," *Science*, vol. 317, no. 5845, pp. 1698-1702, Sep. 2007.
- [15] N. Engheta, A. Salandrino, and A. Alù, "Circuit elements at optical frequencies: Nanoinductors, nanocapacitors, and nanoresistors," *Physical Review Letters*, vol. 95, no. 9, pp. 095504/1-4, August 2005.
- [16] A. H. Panaretos, Y. A. Yuwen, D. H. Werner, and T. S. Mayer, "Tuning the optical response of a dimer nanoantenna using plasmonic nanoring loads," *Scientific Reports*, vol. 5, no. 1, pp. 9813-9826, May 2015.
- [17] A. Alù and N. Engheta, "Input impedance, nanocircuit loading, and radiation tuning of optical nanoantennas," *Physical Review Letters*, vol. 101, no. 4, pp. 043901/1-4, July 2008.
- [18] K. Iizuka, "The circular loop antenna multiloaded with positive and negative resistors," *IEEE Trans. Antennas Propag.*, vol. 13, no. 1, pp. 7-20, Jan. 1965.
- [19] R. L. Li, N. Bushyager, J. Laskar, and M. M. Tentzeris, "Circular loop antennas reactively loaded for a uniform traveling-wave current distribution," *2005 IEEE Antennas and Propagation Society International Symposium*, 2005, pp. 455-458 vol. 3B.
- [20] H. Iizuka, P. S. Hall, "Omnidirectional left-handed loop antenna," *2006 IEEE Antennas and Propagation Society International Symposium*, July 2006.
- [21] D. Ahmadian, Ch. Ghobadi and J. Nourinia, "Ultra-compact two-dimensional plasmonic nano-ring antenna array for sensing applications," *Optical and Quantum Electronics*, vol. 46, no. 9, pp. 1097-1106, 2014.
- [22] A. F. McKinley, T. P. White, and K. R. Catchpole, "Designing nano-loop antenna arrays for light-trapping in solar cells," *Photovoltaic Specialists Conference (PVSC)*, pp. 1894-1896, 2013.
- [23] MATLAB R2014A, Mathworks - Natick, MA, USA, <https://www.mathworks.com/>
- [24] FEKO Suite 7.0, EM Software & Systems - S.A., Stellenbosch, South Africa, <http://www.feko.info>
- [25] Ansys Electronics Desktop 2016, Ansys - Canonsburg, Pennsylvania, USA, <https://www.ansys.com/products/electronics/ansys-hfss>
- [26] T. T. Wu, "Theory of the thin circular loop antenna," *J. Math. Phys.*, vol. 3, no. 6, pp. 1301-1304, 1962.
- [27] A. F. McKinley, T. P. White, I. S. Maksymov, and K. R. Catchpole, "The analytical basis for the resonances and anti-resonances of loop antennas and meta-material ring resonators," *Journal of Applied Physics*, vol. 112, pp. 094911/1-9, 2012.
- [28] D. H. Werner, "An exact integration procedure for vector potentials of thin circular loop antennas," *IEEE Trans. Ant. and Prop.*, vol. 44, pp. 157-165, 1996.

- [29] A. F. McKinley, "Theory of impedance loaded loop antennas and nanorings from RF to optical wavelengths," *IEEE Trans. Ant. and Prop.*, vol. 65, no. 5, pp. 2276-2281, 2017.
- [30] S. V. Savov, "An efficient solution of a class of integrals arising in antenna theory," *IEEE Antennas and Prop. Mag.*, vol. 44, no. 5, pp. 98-101, Oct. 2002.
- [31] T. B. Jones and N. G. Nenad, *Electromechanics and MEMS*. Cambridge University Press, 2013.
- [32] N. Hansen and A. Ostermeier, "Adapting arbitrary normal mutation distributions in evolution strategies: The covariance matrix adaptation," *Proceedings of the 1996 IEEE International Conference on Evolutionary Computation*, pp. 312-317, 1996.
- [33] M. D. Gregory, S. V. Martin, and D. H. Werner, "Improved electromagnetics optimization: The covariance matrix adaptation evolutionary strategy," *IEEE Antennas and Propagation Magazine*, vol. 57, no. 3, pp. 48-59, 2015.
- [34] M. D. Gregory, Z. Bayraktar, and D. H. Werner, "Fast optimization of electromagnetic design problems using the covariance matrix adaptation evolutionary strategy," *IEEE Transactions on Antennas and Propagation*, vol. 59, no. 4, pp. 1275-1285, 2011.
- [35] K. Deb, *Multi-Objective Optimization Using Evolutionary Algorithms*. Chichester, UK: John Wiley and Sons, 2001.
- [36] D. Hadka and P. Reed, "Borg: An auto-adaptive many-objective evolutionary computing framework," *Evolutionary Computation*, Vol. 21, No. 2, pp. 231-259, DOI:10.1162/EVCO.a.00075.
- [37] J. Nagar and D. H. Werner, "A comparison of three uniquely different state of the art and two classical multiobjective optimization algorithms as applied to electromagnetics," *IEEE Transactions on Antennas and Propagation*, vol. 65, no. 3, pp. 1267-1280, 2017.
- [38] R. C. Hansen, *Electrically Small, Superdirective and Superconducting Antennas*. New York, USA: John Wiley and Sons, 2006.
- [39] H. A. Wheeler, "Fundamental limitations of small antennas," *Proceedings of the IRE*, vol. 35, no. 12, pp. 1479-4784, 1947.
- [40] L. J. Chu, "Physical limitations of omni-directional antennas," *J. Appl. Phys.*, vol. 19, no. 12, pp. 1163-1175, 1948.
- [41] W. Geyi, "Physical limitations of antenna," *IEEE Transactions on Antennas and Propagation*, vol. 51, no. 8, pp. 2116-2123, 2003.
- [42] B. Q. Lu, J. Nagar, T. Yue, M. F. Pantoja, and D. H. Werner, "Closed-form expressions for the radiation properties of nanoloops in the terahertz, infrared and optical regimes," *IEEE Trans. Antennas Propag.*, vol. 65, no. 1, pp. 121-133, 2017.
- [43] M. F. Pantoja, J. Nagar, B. Q. Lu, and D. H. Werner, "Existence of superdirective radiation modes in thin-wire nanoloops," *ACS Photonics*, vol. 4, no. 3, pp. 509-516, 2017.
- [44] J. Nagar, S. D. Campbell, P. L. Werner, and D. H. Werner, "Multi-objective tradeoff studies of directivity achievable by electrically small nanoloops," *2017 URSI GASS*, 2017, pp. 1-4.
- [45] J. Nagar, S. D. Campbell, Q. Ren, J. A. Easum, R. P. Jenkins, and D. H. Werner, "Multi-objective optimization aided metamaterials-by-design with application to highly directive nano-devices," *IEEE Journal on Multiscale and Multiphysics Computational Techniques*, vol. 2, no. 1, pp. 147-158, 2017.
- [46] J. Nagar, B. Q. Lu, M. F. Pantoja, and D. H. Werner, "Analytical expressions for the mutual coupling of loop antennas valid from the RF to optical regimes," *IEEE Transactions on Antennas and Propagation*, vol. 65, no. 12, pp. 6889 - 6903, Dec. 2017.
- [47] J. M. Liu, *Photonic Devices*. Cambridge: Cambridge University Press, 2005.
- [48] R. Li, N. A. Bushyager, J. Laskar, and M. M Tentzeris, "Determination of reactance loading for circularly polarized circular loop antennas with a uniform traveling-wave current distribution," *IEEE Transactions on Antennas and Propagation*, vol. 53, no. 12, pp. 3920-3929, 2005.



Jogender Nagar received the B.S. degree in electrical and computer engineering from the Ohio State University in 2008 and the M.S. from Johns Hopkins in electrical and computer engineering in 2011. He is currently a member of the Computational

Electromagnetics and Antennas Research Lab (CEARL) at the Pennsylvania State University in University Park, PA where he is working towards his Ph.D. His work experience includes two years at Northrop Grumman in Linthicum Heights, MD as an antenna systems engineer.

His research interests include computational electromagnetics, antenna theory and design, transformation optics, gradient-index lens design, multi-objective optimization, and nanoantennas.



Ryan J. Chaky received the B.S. degree in electrical engineering from Bucknell University in 2017. He is currently pursuing a Ph.D. at the Pennsylvania State University as a member of the Computational Electromagnetics and Antennas Research Lab (CEARL). His research interests include antenna theory and design, nanoantennas, and metamaterials.



Mario F. Pantoja (M'97-SM'12) received the B.S., M.S., and Ph.D. degree in 1996, 1998, and 2001, respectively, in Electrical Engineering from the University of Granada, Granada, Spain. Since 2004, he has been an Associate Professor at the University of Granada. He has published more than 50 refereed journal articles and book chapters, and more than 100 conference papers and technical reports, and he has participated in more than 40 national and international projects with public and private funding. He was recipient of a 2002 International Union of Radio Science (URSI) Young Scientist Award, and he has received grants to stay as a Visiting Scholar at the Dipartimento Ingegneria dell'Informazione in the University of Pisa, Italy, with the International Research Centre for Telecommunications and Radar at Delft University of Technology, Netherlands, and with the Antenna and Electromagnetics Group at Denmark Technical University. In addition, he has received a Fulbright Grant to collaborate with the Computational Electromagnetics and Antenna Research Laboratory at the Pennsylvania State University, USA.

His research interests include the areas of time-domain analysis of electromagnetic radiation and scattering problems, optimization methods applied to antenna design, Terahertz technology, and nanoelectromagnetics.



Arnold F. McKinley received the master's degrees in engineering-economic systems and electrical engineering from Stanford University, Stanford, CA, USA, in 1973 and 1974, respectively, the master's degree in comparative religions from Graduate Theological Union, Berkeley, CA, USA, in 1989, and the Ph.D. degree from The Australian National University, Canberra, ACT, Australia, in 2014, with a focus on the resonances of nanorings for the use as antennas on solar cells. He was with the Institute for Energy Studies, Stanford, and with the Center for the Study of Social Policy at the Stanford Research Institute (now SRI International), Menlo

Park, CA, USA, in the 1970s. In the early 1980s, he taught at the departments of Physics and Electrical Engineering, San Diego State University, San Diego, CA, USA. For the next 25 years, he was a Professional Programmer on contract and internally for various scientific laboratories and institutions, including Apple Computer, X-Rite Technology, the Minolta Laboratory Systems, and the Center for Research in Mathematics and Science Education. In 1995, he founded MetaMind Software to develop educational software for engineering and science students. He is currently a Teaching Fellow at the Department of Electronics and Electrical Engineering, University College London, London, U.K., where he coordinates the Renewable Energy Minor Program for the Faculty of Engineering, focuses on issues concerned with the integration of renewables on the electrical grid in the U.S., Australia, and Europe, and continues research on nanoring antennas for THz and optical solutions.



Douglas H. Werner received the B.S., M.S., and Ph.D. degrees in electrical engineering and the M.A. degree in mathematics from the Pennsylvania State University (Penn State), University Park, in 1983, 1985, 1989, and 1986, respectively. He holds the John L. and Genevieve H. McCain Chair Professorship in the Pennsylvania State University Department of Electrical Engineering. He is the director of the Computational Electromagnetics and Antennas Research Lab (CEARL: <http://cearl.ee.psu.edu/>) as well as a member of the Communications and Space Sciences Lab (CSSL). He is also a faculty member of the Materials Research Institute (MRI) at Penn State. Prof. Werner was presented with the 1993 Applied Computational Electromagnetics Society (ACES) Best Paper Award and was also the recipient of a 1993 International Union of Radio Science (URSI) Young Scientist Award. In 1994, Prof. Werner received the Pennsylvania State University Applied Research Laboratory Outstanding Publication Award. He was a co-author (with one of his graduate students) of a paper published in the *IEEE Transactions on Antennas and Propagation* which received the 2006 R. W. P. King Award. He received the inaugural *IEEE Antennas and Propagation Society Edward E. Altshuler Prize Paper Award* and the *Harold A. Wheeler Applications Prize Paper Award* in 2011 and 2014 respectively. He also received the *2015 ACES Technical Achievement Award*. He was the recipient of a College of Engineering PSES Outstanding Research Award and Outstanding Teaching Award in March 2000 and March 2002, respectively. He was also presented with an IEEE Central Pennsylvania Section Millennium Medal. In March 2009, he received the PSES Premier Research Award. He is a Fellow of the IEEE, the IET, the OSA, and the ACES.

Prof. Werner is a former Associate Editor of *Radio Science*, a former Editor of the *IEEE Antennas and Propagation Magazine*, an Associate Editor of the *Nature* subjournal *Scientific Reports*, a member of URSI Commissions B and G, Eta Kappa Nu, Tau Beta Pi and Sigma Xi. He holds 14 patents, has published over 750 technical papers and proceedings articles, and is the author of 28 book chapters with several additional chapters currently in preparation. He has published several books including *Frontiers in Electromagnetics*

(Piscataway, NJ: IEEE Press, 2000), *Genetic Algorithms in Electromagnetics* (Hoboken, NJ: Wiley/IEEE, 2007), *Transformation Electromagnetics and Metamaterials: Fundamental Principles and Applications* (London, UK: Springer, 2014), *Electromagnetics of Body Area Networks: Antennas, Propagation, and RF Systems* (Hoboken, NJ: Wiley/IEEE, 2016), and *Broadband Metamaterials in Electromagnetics: Technology and Applications* (Pan Stanford Publishing, 2017). He has also contributed chapters for several books including *Electromagnetic Optimization by Genetic Algorithms* (New York: Wiley Interscience, 1999), *Soft Computing in Communications* (New York: Springer, 2004), *Antenna Engineering Handbook* (New York: McGraw-Hill, 2007), *Frontiers in Antennas: Next Generation Design and Engineering* (New York: McGraw-Hill, 2011), *Numerical Methods for Metamaterial Design* (New York: Springer, 2013), *Computational Electromagnetics* (New York: Springer, 2014), *Graphene Science Handbook: Nanostructure and Atomic Arrangement* (Abingdon, Oxfordshire, UK: CRC Press, 2016), *Handbook of Antenna Technologies* (New York: Springer, 2016), and *Transformation Wave Physics: Electromagnetics, Elastodynamics and Thermodynamics* (Boca Raton, FL: CRC Press, 2016).

His research interests include computational electromagnetics, antenna theory and design, phased arrays (including ultra-wideband arrays), microwave devices, wireless and personal communication systems (including on-body networks), wearable and e-textile antennas, RFID tag antennas, conformal antennas, reconfigurable antennas, frequency selective surfaces, electromagnetic wave interactions with complex media, metamaterials, electromagnetic bandgap materials, zero and negative index materials, transformation optics, nanoscale electromagnetics (including nanoantennas), fractal and knot electrodynamics, and nature-inspired optimization techniques (genetic algorithms, clonal selection algorithms, particle swarm, wind driven optimization, and various other evolutionary programming schemes).